Accurate and computationally efficient third-nearest-neighbor tight-binding model for large graphene fragments

Sören Wohlthat,[1] Jeffrey R. Reimers,[1] and Noel S. Hush[1,2]
[1]*School of Chemistry, The University of Sydney, Sydney, New South Wales 2006, Australia*
[2]*School of Molecular and Microbial Biosciences, The University of Sydney, Sydney, New South Wales 2006, Australia*
(Received 29 January 2010; revised manuscript received 1 April 2010; published 26 May 2010)

Owing to the large sizes involved, most calculations of the electronic properties of graphene and its fragments involve empirical tight-binding models restricted to nearest-neighbor interactions only. Such approaches fail to predict key electronic and magnetic properties, however, and rely on assumed geometries. While alternative approaches based on density-functional theory are much more successful in predicting properties, they are often computationally prohibitive to apply. We introduce a simple third-nearest-neighbor π-only tight-binding approach that maintains the computational efficiency of the empirical method while achieving the accuracy of the density-functional methods to which it is parametrized. It yields both nuclear geometries and electronic structures of graphene fragments, providing an efficient and accurate replacement for traditional tight-binding models of graphene.

DOI: 10.1103/PhysRevB.81.195125 PACS number(s): 73.22.Pr, 72.80.Vp, 61.48.Gh

I. INTRODUCTION

Until its fabrication a few years ago,[1] graphene was considered a starting point for theoretical investigations of graphite, fullerenes, and carbon nanotubes. Since, graphene has become a promising research topic in its own right.[2,3] Apart from graphene's potential for technological applications,[2,4,5] a most intriguing aspect is that its electronic structure around the Fermi energy can be approximated by the Dirac equation for massless particles.[6,7] Thus effects known from quantum electrodynamics have counterparts in graphene.[5] The most common way to derive the approximated Dirac equation is to start from a first-nearest-neighbor tight-binding (TB) (Hückel) model.[3] The nearest-neighbor-only model gives a linear dispersion relation at the Fermi energy[3,8]

$$E(\vec{q})_{\pm} \approx \pm v_F|\vec{q}|, \tag{1}$$

where the momentum $\vec{q}$ is measured with respect to the corners of the Brillouin zone and the Fermi velocity is $v_F = 3d/2t_1$, with t_1 the nearest-neighbor coupling and d the nearest-neighbor distance. If interactions up to third-nearest neighbors are included, the dispersion relation is still linear around the Fermi energy but the Fermi velocity is $v_F = 3d/2(t_1 - 2t_3)$, where t_3 is the third-nearest-neighbor (3nn) coupling.[9] However, away from the Fermi energy the agreement between the nearest-neighbor-only tight-binding and density-functional theory (DFT) π bandstructures is rather poor. Interactions up to third-nearest neighbors are necessary to reproduce the DFT calculations accurately over the entire Brillouin zone.[10]

While for infinitely extended graphene the first-nearest-neighbor model gives in principle the same result as the third-nearest-neighbor model in the vicinity of the Fermi energy, this is not the case if the sheets are truncated. The electronic structure around the Fermi energy depends markedly on the boundaries associated with the edges of these graphene fragments or ribbons and changes significantly with the specific tight-binding model employed. Thus in the single-parameter nearest-neighbor-only tight-binding model infinite armchair ribbons of width $3m-1$ with m an integer are metallic.[11] The same ribbons, however, have band gaps if DFT is employed.[12] The optimized geometries show a shortening of the bond length between hydrogen passivated carbon atoms along the armchair edge by roughly 3.5%. Empirically incorporating these changes in bond length by increasing the corresponding nearest-neighbor coupling by 12% opens a band gap.[12] However, it might not be straightforward to apply the changes in the coupling to more complex geometries.

That the distortion is not the only effect influencing the band gap was shown by White *et al.*[9] Their calculations of the electronic structure of $3m-1$ armchair ribbons with all distances set to the same length display no metallic character. They show that formation of an energy gap can be obtained by inclusion of third-nearest-neighbor interactions in the model. Nevertheless, the authors state that it makes little difference whether the interactions are included explicitly or simply absorbed into an effective nearest-neighbor coupling in the tight-binding band structure of zigzag-edge ribbons. On the contrary, examining band structures of non-Peierls' distorted polyacene (the smallest zigzag ribbon), there is an obvious difference between nearest-neighbor-only and long-range neighbor-interaction models.[13,14] In the nearest-neighbor-only model the asymmetric π band and the symmetric π^* band become degenerate at the Fermi energy while in the third-nearest-neighbor model they cross each other. This crossing has a profound effect on the influence of onsite defects in polyacene, as we will show in the end of the paper. Instead of having a vanishing conductance at the Fermi energy due to the defect,[15] the effect is a rather minor change in the conduction properties.

Although shortcomings of the single-parameter tight-binding model are well known, they are often applied to graphene ribbons, ignoring that better tight-binding methods to calculate the geometry and electronic structure of these graphene ribbons do exist [Naval Research Laboratory Tight-Binding (NRL-TB) (Refs. 16 and 17) and density functional

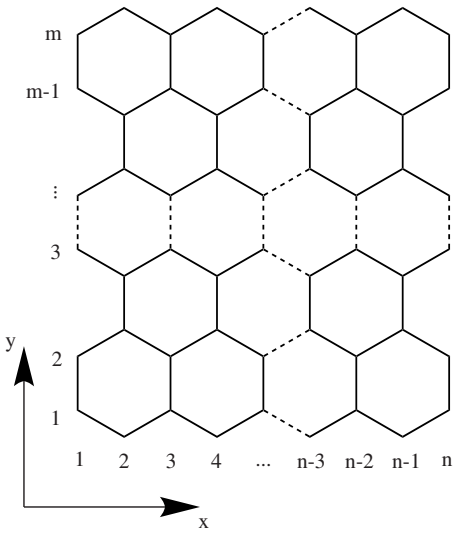

FIG. 1. Sketch of the graphene sheets. The sheets are given as $m \times n$, where m is the number of zigzag rows and n the number of carbon atoms per zigzag row.

based tight binding (DFTB) (Ref. 18)]. Therefore, the question to be answered is, why these methods are not used widely. One of the reasons might be that the aforementioned methods use nonorthogonal basis sets to increase the transferability of the parameters to other systems, making them harder to interface to analytical approaches. Another might be the inclusion of unimportant σ orbitals, making the methods more computationally demanding than is essential. Here, we set out to describe a simple self-consistent orthogonal tight-binding (Hückel-type) model, similar to models successfully applied to conjugated hydrocarbons in the early stages of quantum chemistry.[19]

II. EXTRACTING AN EFFECTIVE π SYSTEM FROM DFT

To develop the method, we start by analyzing DFT calculations of rectangular hydrogen terminated graphene sheets. We therefore optimize the geometry and electronic structure of ferromagnetic (FM) and antiferromagnetic (AFM) 8×17 and 10×19 graphene sheets with four unpaired spins. A sketch of the sheets is given in Fig. 1. The optimization is done with TURBOMOLE (Ref. 20) in a split valence plus polarization (SVP) basis set.[21] The density functional used is BP86.[22,23] We further use the resolution of the identity (RI) approximation.[24,25]

The electronic properties of graphene are dominated by the π system around the Fermi energy. Hence, we extract the π system from the full Hamiltonian. We Löwdin orthogonalize[26] the corresponding π Hamiltonian and obtain its eigenvector coefficients $\tilde{c}_{ik}$ to construct the full-valence density matrix for the individual spins σ,

$$\tilde{p}_{ij}^{\sigma} = \sum_{k}^{\text{valence}} \tilde{c}_{ik}^{\sigma} \tilde{c}_{jk}^{\sigma}. \tag{2}$$

i and j indicate the basis function and k the molecular orbital. Since we are interested in all states around the Fermi energy, not just the occupied ones, we sum over all occupied and virtual valence orbitals and exclude only the Rydberg orbitals. We then transform the Hamiltonian into a natural atomic-orbital basis[27] corresponding to the full-valence density matrix. We therefore diagonalize the blocks of the full-valence density matrix corresponding to individual atoms and use the same transformation to change the basis of the π Hamiltonian. We partition the system into a minimal valence basis and a Rydberg basis according to the occupation of the natural orbitals. By using the partitioning technique of Larsson,[28] we incorporate the influence of the π Rydberg states on the minimal π basis and thus produce an effective π Hamiltonian in a minimal basis.

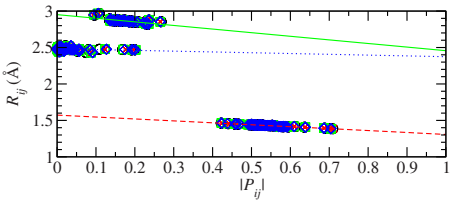

FIG. 2. (Color online) Bond length R_{ij} vs absolute values of the bond order P_{ij} between atoms i and j for a 10×19 graphene sheet and a 8×17 graphene sheet extracted from DFT. The results for the ferromagnetic 10×19 graphene sheet are indicated by black circles, the ones for the antiferromagnetic 10×19 sheet are shown as red crosses. Green squares correspond to the ferromagnetic 8×17 sheet and blue diamonds to the antiferromagnetic 8×17 sheet. The lines are linear fits for first-, second-, and third-nearest neighbors. The red dashed line is the fit to the first-nearest neighbors (R_{ij}=1.5729 Å−0.26538 Å$|P_{ij}|$). The blue dotted line is the fit to the second-nearest neighbors (R_{ij}=2.4828 Å−0.10867 Å$|P_{ij}|$). The green solid line is the fit to the third-nearest neighbors (R_{ij}=2.9511 Å−0.49474 Å$|P_{ij}|$).

III. BOND ORDER TO BOND-LENGTH CORRELATION

From the Hamiltonian matrix in this effective π basis, we calculate the (actual) density matrix for α and β spins

$$p_{ij}^{\sigma} = \sum_{k} \nu_k^{\sigma} c_{ik}^{\sigma} c_{jk}^{\sigma}, \tag{3}$$

using the occupancy ν_k of molecular orbital k. Those elements that connect two different atoms i and j (the off-diagonal elements of the density matrix) are the total bond orders of spin σ. The total bond order between two atoms is the sum of the individual spin components $p_{ij}=p_{ij}^{\alpha}+p_{ij}^{\beta}$. For example, the bond order for a nearest-neighbor bond in infinite graphene has previously been calculated to be 0.525.[29,30] For conjugated hydrocarbons, the bond lengths R_{ij} are approximately linearly dependent on the total bond orders $P_{ij}=p_{ij}^{eq}$ for equilibrium geometries.[19,31–33] Thus, we plot the sum of the moduli of the bond orders of α and β spins against the interatomic distance for graphene sheets up to third-nearest neighbors in Fig. 2. Linear regression gives for first-nearest neighbors

$$R_{ij} = 1.5729 \text{ Å} - 0.26538 \text{ Å}|P_{ij}|, \tag{4}$$

for second-nearest neighbors

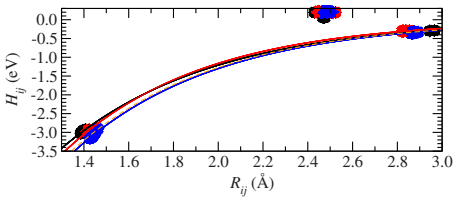

FIG. 3. (Color online) Couplings H_{ij} vs interatomic distance R_{ij} of ferromagnetic and antiferromagnetic graphene sheets of size 10×19 and 8×17 with atoms i and j. Couplings between atoms each having two nearest neighbors (2-2) are shown in black. Couplings between one atom with two nearest neighbors and one with three nearest neighbors (2-3) are colored in red. Couplings between atoms each having three nearest neighbors (3-3) are blue. The lines are exponential fits to the first- and third-nearest-neighbor interactions of the different sets. The symbols indicating the individual sets are listed in the supplementary data (Ref. 34). The fit to the combined data is shown as a dotted orange line.

$$R_{ij} = 2.4828 \text{ Å} - 0.10867 \text{ Å}|P_{ij}|, \tag{5}$$

and for third-nearest neighbors

$$R_{ij} = 2.9511 \text{ Å} - 0.49474 \text{ Å}|P_{ij}|. \tag{6}$$

The relations for the individual sheets are listed in the supplementary information;[34] these relationships reflect the basic topology of conjugated hydrocarbons.

The relation for first-nearest neighbors given by Coulson and Golibiewski[31] in 1961

$$R_{ij} = 1.517 \text{ Å} - 0.180 \text{ Å}|P_{ij}| \tag{7}$$

was obtained by fitting to experimental measurements of bond lengths of ethylene, benzene, and graphite and varies somewhat from the one obtained here from DFT calculations of graphene sheets. A similar linear relation also in common use[35] is due to Dewar and Gleicher.[36] Our relation [Eq. (4)] gives a rather large value of 1.573 Å for the single bond as compared to these results and, for example, to the observed C-C distance in ethane, 1.536 Å.[37] Applied to benzene, where the bond order is 2/3 and thus the bond length determined from Eq. (4) would be 1.396 Å, which is in good agreement with the experimental value of 1.397 Å.[38] The bond length of infinite graphene is perceived to be 1.434 Å again close to the experimental nearest-neighbor bond length of 1.422 Å in graphite.[39] Our relationship also underestimates the double bond length in ethylene, 1.308 Å compared to the observed value of 1.339 Å. Hence the method works very well for intermediate-strength bonds typical of graphene fragments but slightly overestimates single bond lengths and slightly underestimates double bond lengths.

IV. COUPLINGS

In Fig. 3, we plot the coupling (also called resonance integral or hopping) against the interatomic distance. Examining the results, it is obvious that the absolute values of the second-nearest-neighbor couplings are smaller than the third-nearest-neighbor ones. This is an effect of the geometry manifesting itself through the orthogonalization of the DFT Hamiltonian.

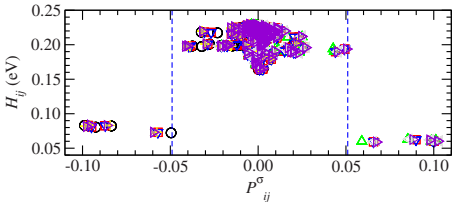

FIG. 4. (Color online) Second-nearest-neighbor couplings vs the spin component of the bond order. The individual symbols are given in the Supplementary Information (Ref. 34). The vertical dashed blue lines point up where the steps appear.

By fitting the first-nearest-neighbor couplings as exponentially decreasing with distance, we have noticed that the third-nearest-neighbor couplings correlate well. Thus, we include the third-nearest-neighbor interactions in the fits shown in Fig. 3. We further classify the couplings by the number of nearest neighbors of the atoms connected by the coupling element. Since carbon atoms in graphene sheets have either two or three first-nearest-neighbor carbon atoms, we get three different combinations. Fits to the individual sets are shown in the figure and their functions are given in the supplementary information.[34] Our main goal, however, is to keep the parametrization as simple as possible and we, therefore, fit all the first- and third-nearest-neighbor couplings to a single exponential, which is shown as the dashed line in Fig. 3. The function describing the fit to all of the data is

$$H_{ij} = -27.973 \text{ eV } e^{-1.5463/\text{Å } R_{ij}}. \tag{8}$$

This relation is put into its historic context in the Appendix.

The second-nearest-neighbor couplings can be separated into two different categories. The couplings between atoms with two nearest neighbors along the zigzag edge are around +0.08 eV for α spins and around +0.06 eV for β spins in the ferromagnetic case while all other second-nearest-neighbor couplings are around +0.2 eV. Notice that these couplings enter with a positive sign. We plot the second-nearest-neighbor couplings directly as a function of the bond order in Fig. 4. The bond order connecting two neighboring zigzag-edge atoms is for α spins lower than −0.049 and for β spins larger than 0.051.

V. ONSITE ENERGIES

Starting from the Pople-Nesbet equations[40] in an orthogonal atomic π-orbital basis

$$H^{\sigma}C^{\sigma} = C^{\sigma}\varepsilon^{\sigma}, \tag{9}$$

we can approximate the diagonal Hamiltonian matrix elements by neglecting all but those orbitals coming from the same spatial orbital χ. Thus we get

$$\alpha^{\sigma} = H^{\sigma}_{\mu\mu} \approx \alpha_0 - \omega(0.5 - q^{\sigma'}_{\mu}) \tag{10}$$

with

$$\alpha_0 = H^{1}_{\mu\mu} + 0.5\omega,$$

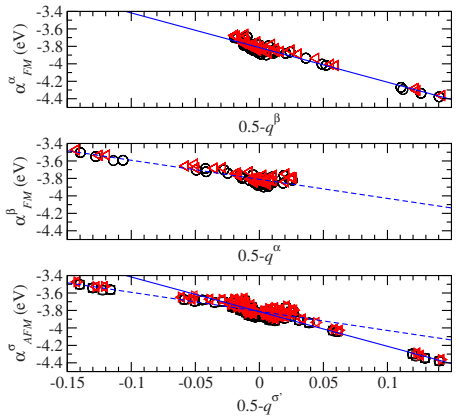

FIG. 5. (Color online) Onsite energy α of the π orbital of spin $\sigma=\alpha,\beta$ vs 0.5 minus the spin component of the π electron density $q^{\sigma'}$ of spin $\sigma'=\beta,\alpha$ with $\sigma\neq\sigma'$ for FM and AFM graphene sheets of size 10×19 and 8×17. The results for the 10×19 sheet are displayed as black circles except the AFM β spins (black squares). The results for the 8×17 sheet are plotted as left pointing triangles with the exception of the AFM β spins (red right pointing triangles). The blue solid line is a linear fit to the FM results of α spin of both sheets. The blue dashed line is this fit to FM β spins. The FM fits are also shown in the diagram of the AFM onsite energies to highlight that the AFM onsite energies fall on the same lines.

$$\omega = \int d^3r_1 \int d^3r_2 \chi^*_\mu(\vec{r}_1)\chi^*_\mu(\vec{r}_2)\frac{1}{r_{12}}\chi_\mu(\vec{r}_1)\chi_\mu(\vec{r}_2),$$

the one-electron integrals $H^1_{\mu\mu}=\int d^3r_1 \chi^*_\mu(\vec{r}_1)H(\vec{r}_1)\chi_\mu(\vec{r}_1)$, and $\sigma\neq\sigma'$. The electron densities q^σ_μ are the diagonal elements of the density matrix. If we treat α_0 and ω as parameters, then the approximation is similar to the "ω approximation" commonly used in semiempirical electronic-structure theories.[19,41,42] To get the parameters α_0 and ω from DFT, we plot the onsite energies of spin σ against the local densities of spin σ', which we extracted from the effective π Hamiltonian in Fig. 5. The results for FM and AFM sheets of size 10×19 and 8×17 are displayed in Fig. 5. For the FM sheets, the fit to the onsite energies of the majority spins α (blue solid line in Fig. 5) is

$$H^\alpha_{\mu\mu} = -3.8140\ \text{eV} - 3.9642\ \text{eV}(0.5 - q^\beta) \qquad (11)$$

and to the onsite energies of the minority spins β (blue dashed line in Fig. 5) is

$$H^\beta_{\mu\mu} = -3.8106\ \text{eV} - 2.1842\ \text{eV}(0.5 - q^\alpha). \qquad (12)$$

As can be seen from the bottom panel of Fig. 5, the onsite energies of the AFM sheets can also be approximated by those fits. The information about the individual sheets can again be found in the supplementary information.[34]

The magnetic moment at the edge atoms can be estimated from the figures as well. The difference between the electron density of α and β spins at the zigzag edges is somewhere between 0.2 and 0.3. The magnetization of the edge atoms is therefore in between 0.2 and $0.3\mu_B$, which is consistent with four electrons spread over 16 (8×17 sheet) or 18 (10×19 sheet) zigzag-edge atoms.

It can be anticipated from Fig. 5 that the antiferromagnetic onsite energies α_{AFM} can be approximately obtained from the ferromagnetic ones α_{FM}. This can be achieved for rectangular sheets by applying the following transformation:

$$\alpha^\alpha_{\text{AFM}}(y<0) = \alpha^\alpha_{\text{FM}}(y<0); \quad \alpha^\beta_{\text{AFM}}(y<0) = \alpha^\beta_{\text{FM}}(y<0) \qquad (13)$$

and

$$\alpha^\alpha_{\text{AFM}}(y>0) = \alpha^\beta_{\text{FM}}(y>0); \quad \alpha^\beta_{\text{AFM}}(y>0) = \alpha^\alpha_{\text{FM}}(y>0), \qquad (14)$$

where y is the armchair direction (see Fig. 1) and $y=0$ is in the center of the sheet. A more detailed comparison of the onsite energies of the 10×19 graphene sheet is shown in the supplementary information.[34] The approximation is very good at the edges. However, the values for the onsite energies of the ferromagnetic sheet are somewhat closer to the average value than the ones of the antiferromagnetic sheet in the vicinity of the center.

VI. GEOMETRY OPTIMIZATION

The calculation starts from an initial coordinate file and sets up an initial Hamiltonian. The onsite energies are determined from Eqs. (11) and (12). The couplings between first- and third-nearest neighbors are calculated from Eq. (8). The couplings between second-nearest neighbors are +0.02 eV in the initial step.

From this initial Hamiltonian the bond order and electron density are calculated. By applying the bond-order bond-length correlations [Eqs. (4)–(6)], the bond orders are turned into distances. Since we have distances between up to third-nearest neighbors, the geometry of a graphene sheet is generally overdetermined. Therefore, we perform a least-squares fit of the coordinates of the atoms to the distances. We weigh the first-nearest-neighbor distances a factor of 10 higher than the second- and third-nearest-neighbor distances. From the fitted set of coordinates the new Hamiltonian is created. However, this time the second-nearest-neighbor couplings are varied if the bond order is lower than −0.049 to +0.08 eV and if the bond order is greater than 0.051 to +0.06 eV. This procedure is iterated until no matrix element of the Hamiltonian changed by more than 10^{-4} eV. In order to achieve a faster convergence the bond order is damped.

VII. APPLICATION

To test the third-nearest-neighbor model described above, we optimize the geometry of a 10×11 graphene sheet with DFT, DFTB, and with the third-nearest-neighbor model and compare the respective bond lengths. The results are summarized in Table I. To allow for a fair comparison between the tight-binding schemes, we calculated the sheet with functionals and basis sets that enter into the different schemes. Since we are using DFTB with parameters from the "mio-0-1" Slater-Koster files, the PBE (Ref. 43) functional enters as the basis for the parametrization while B3LYP (Refs. 22, 44, and 45) together with the 6-31G* basis set[46] enters through the

TABLE I. Comparison of the nearest-neighbor bond lengths of a 10×11 graphene sheet calculated with different methods. The largest deviation is found by comparing different DFT calculations (PBE/SVP and B3LYP/6-31G*). The error coming from the approximations inherent in the tight-binding schemes is therefore smaller than the uncertainty stemming from the implementations of DFT. σ_{bl} is the standard deviation of the bond lengths. 3nn is the third-nearest-neighbor model.

Method 1	Method 2	σ_{bl} (Å)
DFTB/mio-0-1	B3LYP/6-31G*	0.004
DFTB/mio-0-1	PBE/SVP	0.006
3nn	BP86/SVP	0.004
B3LYP/6-31G*	PBE/SVP	0.007
PBE/SVP	BP86/SVP	0.001

parametrization of the repulsive potential. The 3nn method described in this paper was fitted to BP86/SVP results for 8×17 and 10×19 sheets and we see here that it can successfully predict the BP86/SVP results for a 10×11 sheet, the standard deviation of the nearest-neighbor distances being just 0.004 Å. Similarly, DFTB/mio-0-1 successfully reproduces results from the methods used in its parametrization but interestingly slightly overestimates the bond length compared with B3LYP/6-31G* while slightly underestimating those of PBE/SVP (the difference between the generalized gradient approximation functionals PBE/SVP and BP86/SVP is marginal, however). Most significantly, the standard deviation between the B3LYP/6-31G* and PBE/SVP results is 0.007 Å. Thus the uncertainty coming from the DFT functionals is larger than the error of the approximations inherent in either DFTB or the third-nearest-neighbor method described here.

To show that the method gives good agreement not only for graphene fragments but also for other planar hydrocarbons, we compare the bond lengths of some molecules in Fig. 6. The root-mean-square error of the bond length of the third-nearest-neighbor model compared to BP86/SVP for hexabenzocoronene and the molecules shown in Fig. 6 is 0.012 Å. The model gives qualitatively the correct trend of the bond lengths within each molecule. However, localized double bonds are up to 0.038 Å (3%) shorter than in DFT with the butadiene molecules (a, b, and c) being the worst cases. This discrepancy could possibly be reduced by including molecules with localized double bonds in the training set, which consists here only of the 8×17 and 10×19 graphene fragments. Nevertheless our intention is to get an optimized description of graphene fragments, molecules in which bonds are usually highly delocalized.

Another test is the band gap of armchair ribbons. As mentioned in the introduction, single-parameter nearest-neighbor tight-binding models produce qualitatively different results for the energy gap of armchair ribbons than DFT. Here, we will demonstrate that the method described in this work reproduces the gaps calculated with DFT quite accurately. We therefore compare our results to the ones obtained by Son *et al.*[12] in Fig. 7. For comparison, we also include the findings

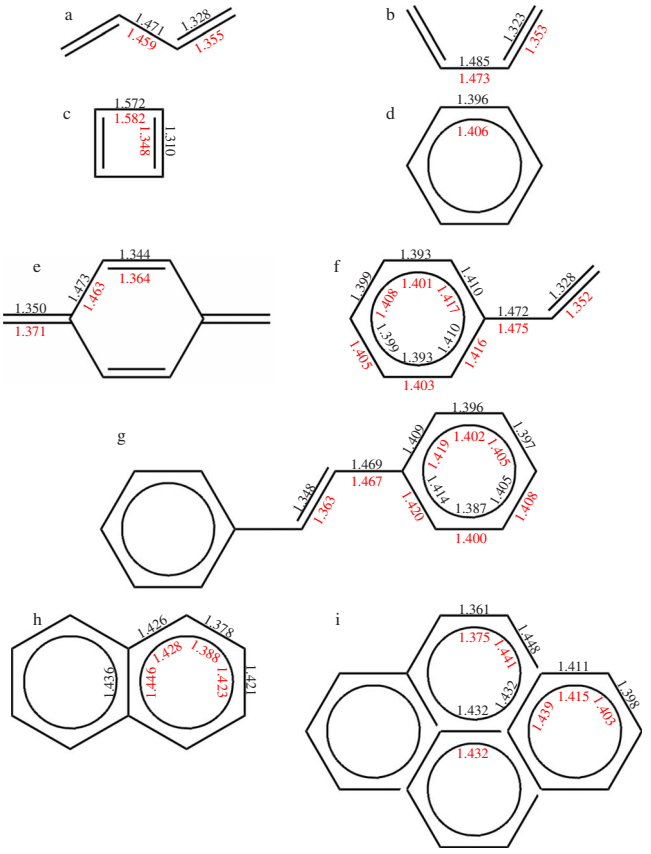

FIG. 6. (Color online) Comparison of bond lengths in Å of small molecules. The (black) results above the bond are obtained with the third-nearest-neighbor model, the (red) numbers below the bonds are calculated with BP86/SVP. The molecules are (a) *trans*-1,3-butadiene, (b) *cis*-1,3-butadiene, (c) cyclobutadiene, (d) benzene, (e) 3,6-bis(methylene)-1,4-cyclohexadiene, (f) styrene, (g) *trans*-stilbene, (h) naphthalene, and (i) pyrene.

of Finkenstadt *et al.*[16] with NRL-TB in the figure. Our results are in very good agreement with the DFT results.

Finally, we investigate polyacene, an example of a zigzag ribbon, calculating its geometrical and electronic structure with DFT and with our third-nearest-neighbor model. The resulting band structures and the associated densities of states are plotted in Fig. 8, along with the band structure from the effective π model and the density of states from the

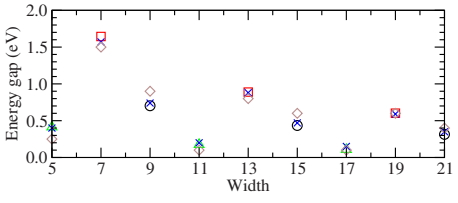

FIG. 7. (Color online) Band gaps of armchair ribbons of varying width calculated with the self-consistent third-nearest-neighbor model. Circles indicate widths of $3m$, squares widths of $3m+1$ and triangles widths of $3m+2$, where m is an integer. The crosses indicate the results obtained by Son *et al.* (Ref. 12) using DFT. The diamonds are the findings of Finkenstadt *et al.* (Ref. 16) using NRL-TB.

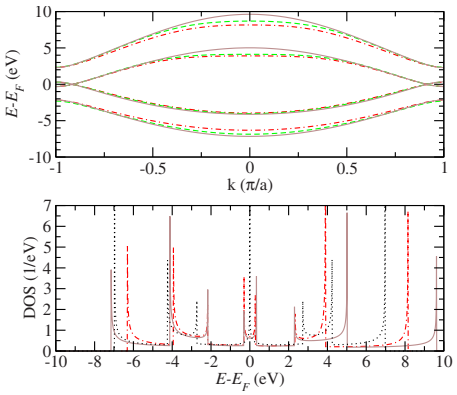

FIG. 8. (Color online) π band structure (top) and associated density of states (bottom) of polyacene calculated with different approximations. The dashed-dotted red lines are the π system extracted from full DFT calculations done with TURBOMOLE (BP86/SVP). The green dashed lines corresponds to the effective π system extracted from the TURBOMOLE data. The solid brown lines are the bands calculated with the third-nearest-neighbor model while the black dots are that as obtained from the nearest-neighbor-only model.

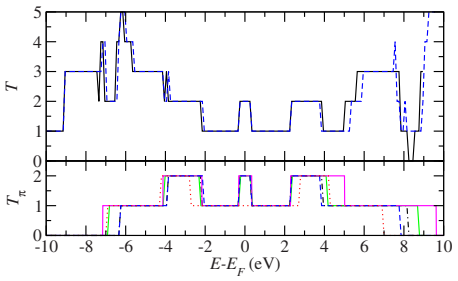

FIG. 9. (Color online) Transmission T of polyacene calculated with different approximations. The top panel displays DFT results for the full system (including contributions from the σ system) calculated with TURBOMOLE (BP86/SVP) (black solid line) and with SIESTA (PBE/DZP) (blue dashed line). The bottom panel displays results of the π system only. The black dashed-dotted line is the transmission through the π system T_π calculated with TURBOMOLE. The blue dashed line is T_π obtained with SIESTA. The green solid line is the effective π system. The solid magenta line is the third-nearest-neighbor model and the red dotted line is the nearest-neighbor-only model. The results are shifted so that the Fermi energy E_F is at 0 eV.

nearest-neighbor-only model. Most significantly, the full π-DFT, effective π-DFT, and 3nn methods agree well around the Fermi energy E_F, with important properties such as the value of the density of states, its derivative (the Fermi velocity), and the location of the nearest resonances being well reproduced; the band widths differ by up to 20%, however, but this inadequacy does not have significant experimental ramifications. At the Fermi energy, the density of states of the nearest-neighbor-only model is qualitatively very different, revealing a profound inadequacy of this overly simplistic approach.

To see the effect of the different methods on the prediction of charge transport properties of polyacene, we apply the Landauer formula,[47] which relates the transmission to the conductance. Thus we need to calculate the transmission through polyacene. We do this by using the wave-function matching method[48,49] with speed ups as discussed by Sørensen *et al.*[50] The transmission of polyacene as predicted by the different methods is displayed in Fig. 9. Since TURBOMOLE has currently no build-in periodic boundary conditions, we extract the necessary information from the central part of a long polyacene (2×33) molecule. To test our procedure against results obtained with periodic boundary conditions, we calculate the transmission of polyacene using SIESTA [PBE density functional using the double zeta plus polarization (DZP) basis set] (Ref. 51) together with the wave-function matching method. We also include results obtained with a single-parameter nearest-neighbor-only tight-binding method to show the deviation of the predictions of this method from all other results. The single-parameter tight-binding method has previously been used by Peres and Sols[15] to calculate the transmission of polyacene.

We notice that the results obtained with SIESTA and TURBOMOLE are very similar. We can further see the effects discussed earlier in the paper. First, the transmission calculated with the third-nearest-neighbor model predicts transmission through the π system in a wider energy range around the Fermi energy than DFT. Second, since the bands cross each other near the Fermi energy in all but the single-parameter nearest-neighbor tight-binding model there is a pronounced region with a transmission of two around the Fermi energy in these models.

We also looked at the influence of a defect in form of a changed onsite energy of the edge atoms of one of the rings in polyacene to compare our results to the ones done with the nearest-neighbor-only tight-binding model in Ref. 15. The transmission for the defective polyacene is shown in Fig. 10. It can be seen that the dramatic effect existent in the single-parameter nearest-neighbor tight-binding model is reduced to a rather weak change in the more sophisticated model.

VIII. CONCLUSIONS

A simple, economic and accurate method is presented for the calculation of the geometry and π electronic structure of H-terminated graphene sheets. It is shown to reproduce the geometry of samples with errors less than the differences in

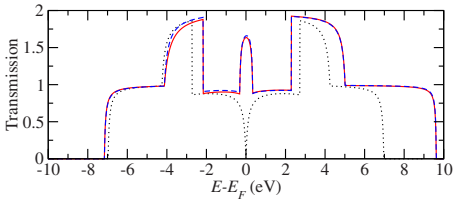

FIG. 10. (Color online) Transmission of polyacene with a defect on the edge atoms of the central ring. The onsite energy was increased by +1.09 eV (0.04 Hartree) in the self-consistent third-nearest-neighbor model (shown as a solid line in red) and in the nearest-neighbor model shown as a dotted black line). The blue dashed line shows a decrease in the onsite energy by −1.09 eV in the self-consistent third-nearest-neighbor model.

the results predicted by commonly used density functionals. The calculated magnetic and electrical properties of the graphene fragments are also found to agree well with those evaluated by density-functional theory, reproducing key properties such as the density of states at the Fermi energy, Fermi velocities, energy differences required for conductance changes, and the probability of electron transmission as a function of incident energy. In particular, the model predicts key features of the density-functional calculations, in agreement with experimental observations, that are not reproduced by simpler nearest-neighbor-only tight-binding approaches in widespread use.[52,53] These results are achieved while maintaining the form and computational efficiency of traditional nearest-neighbor-only models. Hence it provides a fast method for the prediction of useful structural and electronic properties of graphene fragments.

ACKNOWLEDGMENTS

We acknowledge computing resources from the National Computational Infrastructure (NCI) and funding from the Australian Research Council (ARC).

APPENDIX: EXPONENTIAL DEPENDENCE OF THE COUPLINGS ON THE DISTANCE

Historically, the relation between the couplings and the distance was extracted from the a_{1g} and b_{2u} vibration modes of benzene and deuterated benzene by Salem and Longuet-Higgins.[19,54] Based on the assumption of a nearest-neighbor tight-binding model and a nearest-neighbor coupling β exponentially dependent on the distance

$$\beta = \beta(0)e^{-r/a}, \tag{A1}$$

they have found the following relations connecting β to force constants of benzene:

$$k_{a_{1g}} = \frac{2\beta(r_{eq})}{a^2}(P'a) \tag{A2}$$

and

$$k_{b_{2u}} = \frac{2\beta(r_{eq})}{a^2}(P'a + 1). \tag{A3}$$

To compare our fitting procedure to the historic one, we calculate the frequencies of the a_{1g} and b_{2u} vibration modes with DFT and obtain from them the force constants[55,56] needed in the expressions above. For the a_{1g} mode, the computed frequencies of benzene are $\nu_1 = 998.40\ \mathrm{cm}^{-1}$ and $\nu_2 = 3115.47\ \mathrm{cm}^{-1}$. The frequencies of deuterated (d) benzene are $\nu_1^d = 951.40\ \mathrm{cm}^{-1}$ and $\nu_2^d = 2313.12\ \mathrm{cm}^{-1}$. The resulting force constants are $k_1 = 769.22$ N/m, $k_2 = 528.85$ N/m, and $k_{12} = 12.70$ N/m. For the b_{2u} modes, we get $\nu_{14} = 1371.79\ \mathrm{cm}^{-1}$, $\nu_{15} = 1135.56\ \mathrm{cm}^{-1}$, $\nu_{14}^d = 1367.12\ \mathrm{cm}^{-1}$, and $\nu_{15}^d = 806.05\ \mathrm{cm}^{-1}$ for the frequencies. The force constants are $k_{14} = 452.38$ N/m, $k_{15} = 77.58$ N/m, and $k_{1415} = 33.16$ N/m. The frequencies and force constants for the a_{1g} and b_{2u} modes are reasonable.[57,58]

By using the DFT force constants for C_6H_6 and C_6D_6 and the bond order bond-length correlation, we can calculate the exponential dependence of the nearest-neighbor couplings β on the bond length

$$\beta(R) = -35.8297\ \mathrm{eV}\ e^{-1.5521/\text{Å}\,R}. \tag{A4}$$

The equilibrium bond length of 1.396 Å has been used for benzene. The coupling for zero bond length is somewhat larger than the one we obtained from the exponential fit to the first- and third-nearest-neighbor couplings of 10×19 and 8×17 graphene sheets. Although the exponential decay agrees quite remarkably, the idea of a connection between the vibration modes and a self-consistent tight-binding model cannot be trivially generalized to arbitrary molecules within a third-nearest-neighbor model.

[1] K. S. Novoselov, A. K. Geim, S. V. Morozov, D. Jiang, Y. Zhang, S. V. Dubonos, I. V. Grigorieva, and A. A. Firsov, Science **306**, 666 (2004).
[2] A. K. Geim and K. S. Novoselov, Nature Mater. **6**, 183 (2007).
[3] A. H. Castro Neto, F. Guinea, N. M. R. Peres, K. S. Novoselov, and A. K. Geim, Rev. Mod. Phys. **81**, 109 (2009).
[4] M. I. Katsnelson, Mater. Today **10**, 20 (2007).
[5] A. K. Geim, Science **324**, 1530 (2009).
[6] D. P. DiVincenzo and E. J. Mele, Phys. Rev. B **29**, 1685 (1984).
[7] G. W. Semenoff, Phys. Rev. Lett. **53**, 2449 (1984).
[8] P. R. Wallace, Phys. Rev. **71**, 622 (1947).
[9] C. T. White, J. Li, D. Gunlycke, and J. W. Mintmire, Nano Lett. **7**, 825 (2007).
[10] S. Reich, J. Maultzsch, C. Thomsen, and P. Ordejón, Phys. Rev. B **66**, 035412 (2002).
[11] C. A. Coulson and G. S. Rushbrooke, Proc. R. Soc. Edinburgh, Sect. A: Math. Phys. Sci. **62**, 350 (1948).
[12] Y.-W. Son, M. L. Cohen, and S. G. Louie, Phys. Rev. Lett. **97**, 216803 (2006).
[13] M. Kertesz and R. Hoffmann, Solid State Commun. **47**, 97 (1983).
[14] Y. Miyamoto, K. Nakada, and M. Fujita, Phys. Rev. B **59**, 9858 (1999).
[15] N. M. R. Peres and F. Sols, J. Phys.: Condens. Matter **20**, 255207 (2008).
[16] D. Finkenstadt, G. Pennington, and M. J. Mehl, Phys. Rev. B **76**, 121405(R) (2007).
[17] D. A. Papaconstantopoulos, M. J. Mehl, S. C. Erwin, and M. R. Pederson, *Tight Binding Approach to Computational Materials Science*, edited by P. E. A. Turchi, A. Gonis, and L. Colombo, MRS Symposia Proceedings No. 491 (Materials Research Society, Pittsburgh, 1998), p. 221.
[18] M. Elstner, D. Porezag, G. Jungnickel, J. Elsner, M. Haugk, T. Frauenheim, S. Suhai, and G. Seifert, Phys. Rev. B **58**, 7260 (1998).
[19] L. Salem, *The Molecular Orbital Theory of Conjugated Systems*

(W.A. Benjamin, New York, 1966).
[20] R. Ahlrichs, M. Bär, M. Häser, H. Horn, and C. Kölmel, Chem. Phys. Lett. **162**, 165 (1989).
[21] A. Schäfer, H. Horn, and R. Ahlrichs, J. Chem. Phys. **97**, 2571 (1992).
[22] A. D. Becke, Phys. Rev. A **38**, 3098 (1988).
[23] J. P. Perdew, Phys. Rev. B **33**, 8822 (1986).
[24] K. Eichkorn, F. Weigend, O. Treutler, and R. Ahlrichs, Theor. Chem. Acc. **97**, 119 (1997).
[25] K. Eichkorn, O. Treutler, H. Öhm, M. Häser, and R. Ahlrichs, Chem. Phys. Lett. **242**, 652 (1995).
[26] A. Szabo and N. S. Ostlund, *Modern Quantum Chemistry* (Dover, New York, USA, 1996).
[27] A. E. Reed, R. B. Weinstock, and F. Weinhold, J. Chem. Phys. **83**, 735 (1985).
[28] S. Larsson, J. Am. Chem. Soc. **103**, 4034 (1981).
[29] M. Bradburn, C. A. Coulson, and G. S. Rushbrooke, Proc. R. Soc. Edinburgh, Sect. A: Math. Phys. Sci. **62**, 336 (1948).
[30] C. A. Coulson and R. Taylor, Proc. Phys. Soc., London, Sect. A **65**, 815 (1952).
[31] C. A. Coulson and A. Golebiewski, Proc. Phys. Soc. London **78**, 1310 (1961).
[32] R. D. Brown, P. D. Godfrey, B. T. Hart, A. L. Ottrey, M. Onda, and M. Woodruff, Aust. J. Chem. **36**, 639 (1983).
[33] J. E. Gready, J. Comput. Chem. **5**, 411 (1984).
[34] See supplementary material at http://link.aps.org/supplemental/10.1103/PhysRevB.81.195125 for information on individual sheets.
[35] C. F. Wilcox, J. Mol. Struct.: THEOCHEM **759**, 125 (2006).
[36] M. J. S. Dewar and G. J. Gleicher, J. Am. Chem. Soc. **87**, 685 (1965).
[37] G. Herzberg, *Molecular Spectra and Molecular Structure* (Van Nostrand Reinhold, New York, 1966), Vol. 3.
[38] K. Tamagawa, T. Iijima, and M. Kimura, J. Mol. Struct. **30**, 243 (1976).
[39] P. Trucano and R. Chen, Nature (London) **258**, 136 (1975).
[40] J. A. Pople and R. K. Nesbet, J. Chem. Phys. **22**, 571 (1954).
[41] G. W. Wheland and D. E. Mann, J. Chem. Phys. **17**, 264 (1949).
[42] A. Streitwieser, Jr., J. Am. Chem. Soc. **82**, 4123 (1960).
[43] J. P. Perdew, K. Burke, and M. Ernzerhof, Phys. Rev. Lett. **77**, 3865 (1996).
[44] A. D. Becke, J. Chem. Phys. **98**, 5648 (1993).
[45] C. Lee, W. Yang, and R. G. Parr, Phys. Rev. B **37**, 785 (1988).
[46] P. C. Hariharan and J. A. Pople, Theor. Chim. Acta **28**, 213 (1973).
[47] R. Landauer, IBM J. Res. Dev. **1**, 223 (1957).
[48] T. Ando, Phys. Rev. B **44**, 8017 (1991).
[49] P. A. Khomyakov, G. Brocks, V. Karpan, M. Zwierzycki, and P. J. Kelly, Phys. Rev. B **72**, 035450 (2005).
[50] H. H. B. Sørensen, P. C. Hansen, D. E. Petersen, S. Skelboe, and K. Stokbro, Phys. Rev. B **79**, 205322 (2009).
[51] J. M. Soler, E. Artacho, J. D. Gale, A. García, J. Junquera, P. Ordejón, and D. Sánchez-Portal, J. Phys.: Condens. Matter **14**, 2745 (2002).
[52] T. C. Li and S.-P. Lu, Phys. Rev. B **77**, 085408 (2008).
[53] D. A. Areshkin, D. Gunlycke, and C. T. White, Nano Lett. **7**, 204 (2007).
[54] H. C. Longuet-Higgins and L. Salem, Proc. R. Soc. London, Ser. A **251**, 172 (1959).
[55] E. B. Wilson, Jr., J. C. Decius, and P. C. Cross, *Molecular Vibrations: The Theory of Infrared and Raman Vibrational Spectra* (McGraw-Hill, New York, 1955).
[56] B. L. Crawford, Jr. and F. A. Miller, J. Chem. Phys. **17**, 249 (1949).
[57] J. M. L. Martin, P. R. Taylor, and T. J. Lee, Chem. Phys. Lett. **275**, 414 (1997).
[58] L. Goodman, A. G. Ozkabak, and S. N. Thakur, J. Phys. Chem. **95**, 9044 (1991).